Optogenetic strategies for optimizing the performance of biosensors of membrane phospholipids in live cells

Yuanfa Yao[1, #], Xiayan Lou[1, #], Luhong Jin[2], Jianxu, Li[3], Jingfang Liu[2], Yunyue Chen[2], Sunying Cheng[1], Tengjiao Zhao[1], Shuwei Ke[1], Luhao Zhang[2], Peng Zhang[3], Yingke Xu[2, 4*], Lian He[5, *], Hanbing Li[1, *]

1 Institute of Pharmacology, College of Pharmaceutical Science, Zhejiang University of Technology, Hangzhou, 310014, China

2 Department of Biomedical Engineering, Key Laboratory of Biomedical Engineering of Ministry of Education, State Key Laboratory of Modern Optical Instrumentation, Zhejiang Provincial Key Laboratory of Cardio-Cerebral Vascular Detection Technology and Medicinal Effectiveness Appraisal, Zhejiang University, Hangzhou, 310027, China

3 National Key Laboratory of Plant Molecular Genetics, Center for Excellence in Molecular Plant Sciences, Institute of Plant Physiology and Ecology, Shanghai Institutes for Biological Sciences, Chinese Academy of Sciences, Shanghai, 200031, China

4 *Department of Endocrinology, The Affiliated Sir Run Run Shaw Hospital, Zhejiang University School of Medicine, Hangzhou, 310016, China*

5 Department of Pharmacology, School of Medicine, Southern University of Science and Technology, Shenzhen, 518055, China.

# These authors contributed equally: Yuanfa Yao, Xiayan Lou;

*Correspondence should be addressed to **Drs. Hanbing Li**, **Lian He**, and **Prof. Yinek Xu**

Address for Dr. Hanbing Li (lead): Institute of Pharmacology, College of Pharmaceutical Science, 18 Chaowang Road, Zhejiang University of Technology, Hangzhou, 310014, China

Email: hanbing.li@163.com; Tel & Fax: +86-13185064285

Address for Dr. Lian He: Department of Pharmacology, School of Medicine, 1088 Xueyuan Avenue, Southern University of Science and Technology, Shenzhen, 518055, China.

Email: hel3@sustech.edu.cn; Tel & Fax:+86-0755-880100

Address for Prof. Yingke Xu: Department of Biomedical Engineering, 38 Zheda Road, Yuquan Campus, Zhejiang University, Hangzhou, 310027, China

Email: yingkexu@zju.edu.cn ; Tel & Fax: +86-0571-87951091

Abstract

High-performance biosensors are crucial for unraveling the intricate spatiotemporal regulatory roles and dynamics of membrane lipids. However, there remains a significant challenge in improving the sensitivity and substrate detection capabilities of phospholipid biosensors, particularly for low-content substrates. Here we presented universal optogenetic strategies aimed at enhancing a range of membrane biosensors. These strategies involve the precise localization of biosensors within specific membrane regions and following reduction of background signals. Additionally, we introduce an innovative approach utilizing optically-controlled phase separation for the detection and tracking of membrane lipids. The resultant improvements in biosensor performance surpass conventional tools, with the added potential for further enhancement through light simulation. This work not only contributes to the refinement of membrane biosensors but also holds promise for the design and optimization of other biosensor systems.

Introduction

The dynamic metabolism of membrane lipids is a rapid and intricate process that demands high-performance probes for real-time monitoring within living cells. Biosensors play a crucial role in unraveling the spatiotemporal regulatory functions of membrane lipids and have been widely employed to track their fluctuations within cellular environments. A primary optimization approach for enhancing biosensors involves adjusting their sensitivity to specific molecules through the selection of suitable binding motifs from a range of proteins of interest (POI) or the manipulation of binding region copies. In contrast to the pursuit of enhancing biosensor sensitivity, the endeavor to reduced the background signal and further improve their signal-to-noise ratio (SNR) in the imaging process, particularly for membrane phospholipid biosensors with limited sensitivity, has been a relatively unexplored aspect. It is undeniable that the unbound fraction resulting from biosensors

overexpression within cells exerts varying degrees of influence on detection performance, particularly evident with low-abundance tested substrates. In such cases, it may be necessary to implement a 'washing out' process to remove dissociated biosensors as a means to enhance the SNR.

What methods can be employed to more effectively eliminate unbound biosensors and achieve a clearer subcellular visualization of membrane lipid distribution? A more effective strategy to tackle this challenge could involve directing dissociated probes to predetermined non-targeted regions and minimize their impact on the SNR in imaging process. Trapping strategy based on optogenetics is supposed to provide potential solutions by tethering or secluding the unbound probes to other unrelated subcellular structures through photosensitive tool systems, such as LOVTRAP system[1] and LOV2-based nucleocytoplasmic transport system[2, 3]. Optogenetics has found extensive application in manipulating the spatiotemporal localization[4-7] and conformational dynamics of POIs[8], and regulating gene transcription[9-11], modulating ion channel states[12], and facilitating the intracellular movement of organelles[13, 14] in numerous studies. Its high temporal-spatial resolution and reversibility empowers us to intricately manipulate complex cellular processes, leading to a deeper comprehension of the mechanical principles governing both physiological and pathological activities.

The integration of optogenetics into biosensor development and enhancement remains infrequently documented. In pursuit of this objective, our study employed the LOVTRAP system and the LOV2 element to modify a series of membrane lipid biosensors. We sequestered unbound biosensors within cell nucleus or relocated them to unrelated cellular structures under dark conditions. Upon subsequent exposure to light, these stored probes were released, ready to bind to newly synthesized phospholipids in response to agonists. As anticipated, our study demonstrated a reciprocal relationship between the binding and dissociation processes of these improved probes, and the optogenetic transport of biosensors substantially diminished background noise, consequently enhancing the SNR of the biosensors. We applied

these strategies to enhance the functionality of phosphatidic acid (PA), phosphatidylinositol-(3, 4, 5)-trisphosphate (PIP3), and phosphatidylinositol-4-phosphate (PI4P) biosensors. These optogenetics-driven biosensors exhibited superior performance when compared to their non-optimized counterparts. Moreover, to further improve the resolution of biosensors, we used CRY2/CIBN system to optically regulate the phase separation dynamics of Homo-Oligomeric Tag3 (HOTag3) and HOTag6[15-17]. This innovative approach led to a substantial improvement in the detection resolution of the PI4P biosensor. Moreover, this high-resolution biosensor demonstrated the capability to monitor dynamic changes in PI4P levels at the plasma membrane. Collectively, the methodological improvements presented in this study can serve as valuable references for the design of high-performance biosensors and the enhancement of their detection resolution.

Results

Design of optogenetics-based biosensors with the LOVTRAP system

It has been shown that the optogenetics tool CRY2 might affect the behaviors of proteins that fused to its C-terminal, especially for short peptides[18]. We first tested whether this design was suitable for biosensor improvements. The PA biosensor was initially redesigned to address the limitations of existing PA biosensors in accurately detecting PA fluctuations in cells, particularly in cases where most cells exhibit low basal PA levels. Despite the innovative chemical labeling approach devised by the Baskin group to highlight PA levels and indicate PLD activity, the need for improved sensitivity of PA biosensor remained[19-23]. We linked the PA binding protein (PABP) (MDNCSGSRRRDRLHVKLKSLRNKIHKQLHPNCRFDDATKTS) from yeast SPO20 protein to the C-terminus of CRY2 and the resulting CRY2-based PA probe exhibited substantial colocalization with exogenously expressed PLD2. Furthermore, The fusion of two copies of the PABP sequence to CRY2 resulted in an enhanced nuclear localization (**Fig. S1a-b**), suggesting that PABP motifs possess inherent functionality similar to a nuclear localization signal (NLS). Regrettably, the binding of the above probe to PA dose not depend on light stimulation and our design has not

yielded any improvements in the performance of the PA biosensor.

Due to the fact that majority of PA biosensors within cells remain unbound during the basal state, we subsequently explored the LOVTRAP system as a means to sequester these dissociated biosensors within specific regions and release them for PA binding through light stimulation. To achieve this, we first fused the Tom20 to the LOV2 domain and connected PABP to another effector, ZDK1 (**Fig. S1c**). This new construct was termed **Opto**genetics **PA** **S**uper **S**ensor based on **Z**DK/LOV2 (Opto-PASSz). In the dark, the interaction between ZDK1 and LOV2 anchored a significant portion of unbound PA biosensors to the mitochondria (**Fig. S1d**). Upon exposure to light, ZDK1 dissociated from LOV2, leading to the rapid release of the biosensors from the mitochondria (**Fig. S1e**).

Nevertheless, the presence of the mitochondrial network could potentially interfere with the observation of PA changes in other cellular organelles. Therefore, we further opted for the nucleus as a suitable location to sequester the dissociated PA biosensor, given that the inner components of the nucleus are membraneless, with the exception of the nuclear envelope. We connected the histone H2B to LOV2, enabling the recruitment of unbound PA probes into the nucleus in the absence of light (**Fig. 1a**). This binding led to a reduction in background noise in the cytosol, and our Opto-PASSz probe exhibited a low basal PA content in HeLa cells (**Fig. 1b**). Blue light stimulation triggered the dissociation of LOV2 and ZDK, leading to an augmentation in extranuclear fluorescence intensity (**Fig. 1c**). Remarkably, in 293T cells, we observed a significant presence of Opto-PASSz probes on the plasma membrane (**Fig. 1d**). We evaluated the detection performance of PA biosensors by measuring the fluorescence intensity ratio of plasma membrane to the cytoplasm. The results revealed that this ratio surpassed that of the wildly-used PA probe RFP-PASS[21, 23, 24] (**Fig. 1e**). Under conditions where intracellular RFP-PASS expression is high and plasma membrane PA levels are low, Opto-PASSz persistently exhibited a low background signal and had a more substantial enhancement.

Design of optogenetics-based biosensors with circularly permuted LOV2

(cpLOV2)

To broaden the range of biosensors suitable for detecting PA within various subcellular structures, we propose a LOV2-based nucleocytoplasmic transport mechanism for these biosensors. In our previous research, we discovered that the positioning of some phospholipid-binding domains, such as the PABP, at the N-terminal region of LOV2 hindered its binding to PA (data not shown). Consequently, we opted to favor the cpLOV2 variant for the optogenetic modification of membrane lipid biosensors. This preference arised from the exclusive ability of cpLOV2 to accommodate fusion of POIs at the C-terminal.

To accomplish this, we chose seven nuclear export sequences (NES) for fusion with the Jα helix at the N-terminus of cpLOV2. Additionally, we connected a fluorescin (e.g., mCherry) and a nuclear localization sequence (NLS) sequence (e.g., AAAKRSWSMAF) to its C-terminal (**Fig. S2a**). Under the dark condition, the majority of these proteins were localized within the cell nucleus (**Fig. S2b**). After exposure to blue light, two out of the seven tested NES sequences exhibited the expected nuclear export, as originally designed. Among them, the amino acid sequence (DEAAKELAGLDL) demonstrated the highest effectiveness (**Fig. S2a-b**). Subsequently, we conducted a comparative analysis of the binding capabilities of the PABP motif derived from various POIs. Notably, the PABP motifs from yeast overproduction of inositol 1 gene product (Opi1p) and human Raf1 displayed deficiencies in detecting PA levels at the plasma membrane (**Fig. S2c-g**). Consequently, we ultimately incorporated the functionally effective PABP binding motif from SPO20 at the C-terminus of cpLOV2 (**Fig. 2a**). The light-responsive translocation of PA biosensors between the cytosol and the nucleus could potentially impact their affinity for PA. Therefore, we introduced two or more tandem copies of the PA binding region to the cpLOV2. This optogenetics-based PA biosensor was subsequently renamed as **Opto**genetics **PA S**uper **S**ensor based on **c**pLOV2 (Opto-PASSc) (**Fig. 2a**).

The optogenetics-based PA biosensor exhibited a high SNR in cellular PA

imaging

The overexpression of Opto-PASSc in cells predominantly localized to the nucleus (**Fig. 2b**). This localization pattern indirectly indicated a low cytosolic PA content under basal conditions. In a small subset of transfected cells with elevated PA levels, the Opto-PASSc probe distinctly marked the plasma membrane (**Fig. 2b**) and displayed colocalization with RFP-PASS (**Fig. 2c**). Notably, in these cells, the background noise of Opto-PASSc, regardless of its fusion with GFP or mCherry, was lower compared to the referenced PASS probes (**Fig. 2b-d**).

To further enhance the performance of Opto-PASSc, we introduced two mutations (L5A and I14A) to deactivate the function of NES2 (NSNELALKLAGLDINKTE) (**Fig. 2e**). The results of these mutations demonstrated a further reduction in the fluorescence intensity ratio of cytoplasm to the nucleus (**Fig. 2e-f**), which reaffirmed the presence of low PA levels in the majority of cells under non-stimulated conditions. We then investigated whether blue light triggered the unwinding of NES1 within the Jα helix of cpLOV2 and consequently induced Opto-PASSc to translocate into the cytosol. We analyzed the fluorescence intensity ratio of cytoplasm to the nucleus, which increased in response to consecutive blue light illumination (**Fig. 2g**). Of note, Opto-PASSc with NES2 mutations showed an increased export from the nucleus (**Fig. 2g**). Opto-PASSc containing two and four copies of PABPs demonstrated enhanced PA detection at the plasma membrane in comparison to GFP-PASS in HeLa cells (**Fig. 2h**). This superiority persisted when compared to PASS probes harboring an equivalent number of PABP copies in 293T cells. (**Fig. S2h**). Both Opto-PASSc and the previously mentioned Opto-PASSz distinctly labeled PA at the plasma membrane and exhibited equivalent detection performance (**Fig. S2i**). Furthermore, the mutation of four critical basic residues of PABP into glutamic acid, referred to here as PABP 4E mutations, has been previously demonstrated to impair the PA-binding capability. Our results also indicated that Opto-PASSc with PABP 4E mutations was unable to detect an increase in PA at the plasma membrane (**Fig. S2j**). Interestingly, the PABP 4E mutations reduced the nuclear localization of Opto-PASSc (**Fig. S2j**) and led us to

suspect these mutations might influence the NLS-like functionality of the PABP motif. Considering that the aforementioned optogenetic enhancements have demonstrated a promising capacity for improving traditional PA probe PASS, we questioned whether this approach could also be applied to enhance other membrane lipid biosensors. To explore this possibility, we substituted the PA binding motif with the PH domain from the BTK protein for the detection of PIP3 and renamed it as **Opto**genetics **PIP3 S**ensor based on **c**pLOV2 (Opto-PIP3Sc) (**Fig. S3a**). The result indicated that PIP3Sc consistently outperformed the mCh-PHBTK biosensor in detecting insulin-induced PIP3 increases (**Fig. S3a**). A similar enhancement was also evident when redesigning the PI4P biosensor using the previously mentioned strategy (**Fig. S3b** and **Fig. S3c**). Token together, our findings indicate that the cpLOV2-based optogenetic optimization strategy for biosensors may indeed have broader applicability.

Opto-PASSc distinctly labeled PA at the nuclear envelope and demonstrated superior performance in PA labeling compared to PASS under various conditions

Surprisingly, in a subset of HeLa cells expressing Opto-PASSc, the movement of the Opto-PASSc probe between the cytoplasm and the nucleus clearly highlighted the nuclear envelope (**Fig. 3a-b**). A similar phenomenon was also observed in other cell types, such as COS-7 and 293T (**Fig. 3a**). However, it was only when NES2 was in its wild-type state and the expression levels were balanced between the cytosol and nucleus that we could distinctly observe the Opto-PASSc biosensor localizing to the nuclear envelope. To eliminate the possibility that the observed phenotype was a result of frequent shuttling between the cell nucleus and cytoplasm, we co-expressed the green probe Opto-PASSc with wild-type NES2 and the red probe Opto-PASSc with PABP 4E mutations in HeLa cells. The mutated variant of Opto-PASSc was incapable of binding to PA and did not exhibit an increase at the plasma membrane or nuclear envelope, in contrast to Opto-PASSc with wild-type NES2 and PABP (**Fig. 3c**). This finding was consistent with the previously mentioned result (**Fig. S2j**). However, due to the 4E mutations, the NLS-like function of PABP was inhibited, leading to the predominant localization of the Opto-PASSc probe in the cytosol.

Consequently, we co-expressed Opto-PASSc with both wild-type NES2 and PABP, as well as Opto-PASSc with both mutated NES2 and PABP, in HeLa and 293T cells. The unmutated Opto-PASSc exhibited clear labeling of PA at the plasma membrane and nuclear envelope, whereas the mutated probe did not (**Fig. 3c**). Collectively, our results demonstrate that both PABP exclusively located in the cytoplasm and PABP exclusively localized in the nucleus were unable to accurately reflect PA levels at the nuclear membrane. This limitation arises because strong expression either in the cytoplasm or the nucleus can mask the weak signal at the nuclear envelope. The enhanced Opto-PASSc with wild-type NES2 serves as a distinctive biosensor for labeling PA at the nuclear envelope. Unlike other sensors, such as PABP probes derived from Opi1p, Raf1, and PDE4A1[25], which lack this exclusive advantage, the Opto-PASSc biosensor can be employed to investigate the largely-unknown biological functions of PA at the nuclear envelope.

Subsequently, we evaluated the performance of Opto-PASSc in various practical settings for analyzing dynamic changes in PA. As is well-established, in mammals, phospholipase Ds (PLDs) including PLD1, PLD2, and PLD6 are key enzymes that catalyze corresponding lipids such as phosphatidylcholine (PC) or cardiolipin (CL) into PA[26]. Different PLD isoforms have preferential localization, for example, PLD1 primarily resides at the cytosol and perinuclear region, whereas PLD2 predominantly localizes to the plasma membrane, and PLD6 exclusively associates with mitochondria. Besides, the basal activity of PLD2 has been shown higher than that of PLD1[27]. Our initial curiosity revolved around whether Opto-PASSc could accurately depict shifts in PA levels on the plasma membrane. Therefore, we co-expressed PLD2 along with Opto-PASSc or referenced probe PASS and observed that the optimal probe, Opto-PASSc with varying numbers of PABPs, exhibited robust binding to the plasma membrane, regardless of its fusion with GFP or mCherry. This binding was markedly diminished upon inactivation of exogenous PLD2 using either an inactivating mutation (K758R) or the chemical inhibitor FIPI (**Fig. S3d-m**).

Given that the basal activities of endogenous PLDs were typically low, their

activation requires additional stimulation, such as G-protein-coupled receptor agonists and PKC activation. We employed an indirect activator, PMA (a PKC activator), to elevate PA levels at the plasma membrane and evaluated the performance of Opto-PASSc with varying expression intensities in response to drug-induced PA increase in cells. Our results demonstrated that Opto-PASSc outperformed RFP-PASS in tracking PA dynamics at the plasma membrane, regardless of expression level. (**Fig. S4a-c**). The fluorescence intensity ratio of the plasma membrane to the cytoplasm for Opto-PASSc was significantly higher than that of RFP-PASS in the vast majority of analyzed cells, indicating an approximately 1.8-fold improvement with Opto-PASSc. (**Fig. S4c**). In addition, we also found Opto-PASSc more convincingly reflected elevated PA levels at the plasma membrane in 293T cells, in contrast to the conventional PA probe RFP-PASS (**Fig. S4d-e**) and the result from biochemical assay of cellular PLD activities further corroborated the aforementioned observation (**Fig. S4f**), which suggested a potential association between basal PLD activity and cell types.

It has been reported that the cellular PLD1 activity increases after starvation[28, 29]. We thereupon co-expressed RFP-PASS and Opto-PASSc into HeLa cells. Upon four-hour starvation in HEPES buffer, we consistently observed that both RFP-PASS and Opto-PASSc colocalized at the plasma membrane in the majority of the observed cells (**Fig. S4g**). Opto-PASSc distinctly revealed an increase in PA levels at the plasma membrane with a notably higher fluorescence intensity ratio (**Fig. S4g-h**). Moreover, addition of PA binding motif copies also further enhanced the performance of Opto-PASSc (**Fig. S4h**). Unexpectedly, we observed colocalization of RFP-PASS and Opto-PASSc on the endoplasmic reticulum (ER) in a small subset of starved cells (**Fig. S4g**). This phenotype has rarely been reported and remains to be thoroughly elucidated. Collectively, based on the various assessment experiments we conducted, Opto-PASSc probe can more clearly depict changes in PA levels at the plasma membrane. We capitalized on Opto-PASSc to convincedly reveal an increased PA level at the plasma membrane in response to starvation. This finding was in line with

the PA detection achieved through LC-MS methodology[29]. While it has been previously established that PLD1 plays a role in the regulation of autophagy via interactions with various molecules to produce PA[28-30], our results, showing an increase in PA at the plasma membrane, to some extent, suggested the activation of PLD2 under starved stimulation. Other traditional methods, such as biochemical reagents like the Amplex™ Red Phospholipase D Assay Kit or lipidomics techniques (e.g., LC-MS), may encounter challenges when it comes to analyzing PLD isoform activity. In contrast, PA bioimaging using a probe like Opto-PASSc stands out as an effective approach.

To further demonstrate whether the performance of Opto-PASSc depended on light-induced nuclear export, we compared the impact of two treatments, the dark condition and consecutive blue light stimulation at the capture intervals, on the detection ability of Opto-PASSc. Theoretically, light-mediated nuclear export would provide more unbound probe for PMA-induced *de novo* synthesis of PA, which further enhanced fluorescence signal of the plasma membrane. To our expectation, the dissociative probes exported from the nucleus upon pulsing light stimulation at the capture interval (**Fig. S4i**, dotted blue line *v.s.* dotted gray line) and fluorescence intensity ratio (plasma membrane to the cytoplasm) was increased (**Fig. S4i**, solid green line *v.s.* solid gray line). In summary, our results suggested light illumination enhanced the detection performance of Opto-PASSc.

Development of optically-controlled phase separation to enhance the detection resolution of biosensors

Biosensors with high-resolution have the potential to significantly advance our understanding of the specific mechanistic roles of membrane lipids in live cells. In our pursuit of improved detection resolution, we initially explored the SunTag system for single-molecule lipid detection[31]. However, we found the formation of fluorescent clusters might only be controlled by chemical induction and fusion of the lipid binding motif with the SunTag element an adverse impact on affinity (data not shown). Besides, the spontaneous aggregation of the single-chain variable fragment (scFv)

antibody of GCN4 and the huge size of expression system have also discouraged us to improve lipid biosensors. Therefore, to control the formation of fluorescent foci in cells, we capitalized on the interaction-sensitive phase separation of HOTag3/HOTag6 system[15]. HOTag3 can assemble into a hexamer and HOTag6 forms a tetramer. The phase separation would be triggered by the interaction of their fused fragments. By virtue of the light-responsive binding of the optogentic tool CRY2/CIBN, the phase separation process of HOTag3/HOTag6 system became controllable via light stimulation (**Fig. 4a**). Then we added a phospholipid-binding motif, such as P4M domain from SidM, to the CIBN fragment for PI4P detection. In this way, this improved biosensor system generates fluorescent puncta in response to light. The punctum-like probe can bind to intracellular PI4P and it enables us to visually observed the spatial distribution and precise positional information of PI4P more intuitively, which consequently improves its detection resolution in comparison to the sole expression of the fluorescin-fused P4M domain (**Fig. 4a**).

The results were consistent with our expectations. We observed a 10-minute light pulse stimulation induced both green and red puncta in cells (**Fig. 4b**), even after we exchanged the HOTag3 and HOTag6 to the corresponding fused proteins (**Fig. S5a**). To further assess the reversibility of light-induced phase separation, we incubated the stimulated cells in the absence of light for several hours. Our observations revealed that a portion of the phase separation puncta diffused without the presence of light stimulation (**Fig. S5b** and **Fig. 4c**). Given that the disassociation time of CRY2 and CIBN is approximately 10-25 minutes[32], we concluded that the diffusion kinetics of phase separation puncta are primarily determined by the disaggregation of HOTag3 and HOTag6. Our aforementioned result indicated addition of an extra copy of the P4M domain extremely increased its affinity (**Fig. S3b**). Consequently, we fused two copies of the P4M domain with CIBN-HOTag3 or CIBN-HOTag6. The fluorescence intensity of these puncta was approximately 7.32-fold higher than the background signal in the GFP channel (**Fig. 4d** and **Fig. 4f**). Their planar size was approximately 0.240 μm^2 (**Fig. 4e** and **Fig. 4f**), which closely resembled the size of the SunTag foci.

Intriguingly, upon exchanging the fusion of HOTag3 and HOTag6 with their respective optogenetic counterparts (as indicated in the text), there was a modest reduction in both the brightness and size of these puncta (**Fig. 4d** and **Fig. 4e**). We then analyzed the kinetic state of the phase separation spot on the plasma membrane (**Fig. 4f**). Our analysis indicated that the majority of these spots had velocities approximately at 36.6 nm/s (**Fig. 4g** and **Fig. 4h**), a rate significantly lower than the energy-driven translocation speed of kinesin (635-1,290 nm/s) as reported by reference[31]. This dataset suggests that the majority of the spots exhibit modest displacements under the basal state and our probe potentially offer partial insights into the dynamics of PI4P microdomains at the plasma membrane.

Next, we investigated whether this technological improvement enhanced the detection resolution of the PI4P biosensor. Upon subjecting 293T and HeLa cells to approximately 10 minutes of light stimulation, we observed that phase separation puncta were located at the plasma membrane in both red and green channel (**Fig. 4i** and **Fig. 4j**). This observation suggests a notable improvement in detection resolution compared to conventional PI4P biosensors (**Fig. 4i** and **Fig. S5c-d**). When observing the plasma membrane using TIRF microscopy, upon entering critical angle, we can observe an increased number of punctate fluorescent probes on the plasma membrane. (**Fig. 4f** and **Fig. 4j**). Furthermore, these puncta significantly diminished following a half-hour treatment with an inhibitor of PI4P biosynthesis, phenylarsine oxide (PAO) (**Fig. 4j**). The above results suggested that the biosensor based on the optically-controlled phase separation was sufficiently sensitive to capture PI4P changes at the plasma membrane. Its the high detection resolution allows us to track the dynamics of membrane lipids more precisely, facilitating a deeper understanding of specific biological mechanisms.

Discussion

In previous reports and reviews, we highlighted the significant roles of PLDs and PA in cells[26, 33, 34], especially in cancer cells. However, for a more comprehensive understanding of the diverse biological functions of various PLD isoforms and their

real-time activity or dynamics, it requires the use of detection methodologies with enhanced performance. Baskin's group has developed a sophisticated chemical detection platform rooted in click chemistry for the labeling of PA and tracking PLD activities via transphosphatidylation of PLDs[19]. This has empowered us to scrutinize the localization of activated PLDs within subcellular structures[20] and identify cells exhibiting elevated PLD activities[22]. In contrast, the detection of other membrane lipids primarily depends on biosensors, which are developed using truncated binding motifs derived from specific proteins known for their high affinity to these membrane lipids. However, when these probes are individually overexpressed in cells, the presence of unbound biosensors can significantly impact the imaging process, particularly when dealing with low-affinity probes and the detection of low-abundance substrates. Our engineering biosensors, utilizing various optogenetic systems, have been demonstrated to mitigate this interference by sequestering unbound molecules into specific regions. The entire system can be metaphorically compared to the installation of a probe pool within the cell. Unbound probes are housed in this reservoir, minimizing interference in phospholipid imaging. Blue light stimulation functions like turning on the tap of this reservoir, allowing the release of free probes to bind with newly synthesized phospholipids. In dark conditions, the unbound probes return to the probe reservoir, ready for future use. In this system, we need not to concern about the possibility of excessive probe expression levels potentially impacting the imaging process, as it consistently yields a lower background signal and the content of the probe in the target area can be controlled through light. Furthermore, this low-background imaging can also to some extent reflect the baseline levels of the detected phospholipids in the observed region. As expected, we successfully reduced the background signal and improved the SNR in the phospholipid imaging process. Additionally, we uncovered a notable difference: the baseline levels of PA at the plasma membrane of 293T cells were higher than those of HeLa cells. This optogenetics-based improvement has enhanced the performance of PA, PIP3, and PI4P biosensors, ultimately allowing us to more

accurately monitor changes in their levels after various treatments in comparison to non-improved probes.

The light-responsive nucleocytoplasmic transport of the improved biosensors had not only exhibited low background noise but also satisfied the requirements for detecting membrane lipids within cytoplasmic subcellular organelles. Our optimized Opto-PASSc probe, not only exhibited improved detection performance but also unexpectedly allowed us to observe PA levels at the nuclear membrane. Traditional probes are typically expressed exclusively either in the cytoplasm or the nucleus. However, the strong fluorescence signal emitted by these probes can frequently obscure PA levels at the nuclear membrane. This may explain why prior research might have overlooked PA at the nuclear membrane, with only a few studies addressing its role in yeast[35-37]. In mammalian cells, the functions of PA at the nuclear membrane largely remain a mystery. The Opto-PASSc probe developed in this study is poised to play a significant role in future endeavors aimed at analyzing and gaining a deeper understanding of the biological functions of PA at the nuclear membrane. However, we noticed that some lipids-binding motifs themselves had robust nuclear export or import capabilities due to the presence of internal NES or NLS-like amino acid sequences. This presented challenges in the regulation of the probe localization in the basal state by introducing additional screening NES or NLS sequences for the reduction of background signals, particularly in the case of cpLOV2-based strategy. As a result, the LOVTRAP-based strategy emerged as an indispensable solution under such condition because of a highly potent nuclear localization capability of H2B.

The typical membrane lipid biosensors often involve the fusion of fluorescent proteins for visualization. However, most fluorescent proteins are not optimal for enhancing resolution using advanced microscopy techniques such as stochastic optical reconstruction microscopy (STORM) and stimulated emission depletion microscopy (STED). Consequently, the current strategy to address this limitation involves signal amplification through the clustering of multiple fluorescent proteins, as seen in systems like SunTag. This approach has found widespread application in tracking

protein dynamics such as mRNA translation[38, 39]. In our study, we were motivated by the question of whether spot-like phase separation could enhance the detection resolution of biosensors. The combination of HOTag3 and HOTag6, which was identified by Shu's group[15], served as an ideal pair for controlled phase separation. These tags exhibited sensitivity to the interactions between their fused proteins. Our findings indicated that the HOTag3/HOTag6 puncta exhibited similar sizes and dynamics when compared to the SunTag system. Furthermore, the incorporation of optogenetic components CRY2/CIBN into this technique facilitated the initiation of HOTag3/HOTag6-mediated phase separation more effectively. Given that each phase separation punctum was theoretically contains approximately a dozen PI4P-binding motifs P4Ms, it remains uncertain whether an individual phase separation spot corresponds to a single PI4P molecule. We speculated that the number of probe heads for PI4P binding could be regulated by the selection of appropriate HOTags. For example, because HOTag6 forms a tetramer, the cluster formed by the construct consisting of 2×P4M, CIBN, and HOTag6 might have fewer probe heads for PI4P binding compared to the design comprising 2×P4M, CIBN, and the hexameric HOTag3. However, it is undeniable that this optically-controlled phase separation significantly improved the detection resolution of the enhanced PI4P biosensor and our probe partially provided spatial distribution and dynamic information of PI4P microdomains. When using conventional probes, our ability to determine the presence of target phospholipids on the membrane has been limited to qualitative assessments. We evaluate changes in phospholipid levels by monitoring alterations in membrane fluorescence intensity, without access to their specific spatial localization, leading to low-resolution insights. In contrast, our optically-controlled phase separation probe not only provides exceptional brightness, mitigating concerns about photobleaching during extended imaging, but also imparts spatial information regarding the positioning of phospholipid microdomain on the membrane. Moreover, this improved methodology holds promise for future refinements in probes for other metabolites, facilitating precise monitoring of spatiotemporal changes in target substances.

In summary, our study represents an advanced effort in incorporating optogenetic strategies to enhance the functionality of phospholipid biosensors. Compared to the traditional approach in biosensor development, these approaches have increased the molecular size of the probe, which may potentially affect its binding to the target (a concern that can be addressed by increasing the phospholipid-binding copy numbers), as well as has introduced some complexity into the design process. But these optogenetics-based improvements effectively minimized the background signal and thus reflected phospholipids changes in cells more clearly. This has noteworthy implications for refining less effective biosensors currently in use, providing valuable insights for their enhancement. The application of optically-controlled phase separation induced the formation of fluorescent spots, resulting in a substantial increase in the detection resolution of these biosensors. The methodological improvements detailed in this study might serve as a valuable reference for the development of other high-performance, high-resolution biosensors. Such biosensors have the potential to greatly contribute to our understanding of the spatio-temporal dynamics and regulatory roles of membrane lipids in living cells.

Methods

The construction of optogenetics-based biosensors

For CRY2-based sensors, the mcherry-CRY2 was amplified from the mCherry-mCh-CRY2-PR variant[18]. The sequence of mGFP-NES-PABP was amplified from GFP-PASS, a gift from Prof. Guangwei Du. These fragments were subcloned into pLenti-MCS-GFP-SV40-Puro empty vector that linearized by XbaI and SpeI restriction enzymes (New England Biolabs, Inc., USA) via Gibson Assembly kit (TransGen Biotech., China).

For LOVTRAP-based sensors, both the wild type LOV2 and ZDK1 domain were synthesized (Beijing Tsingke Biotech Co., Ltd. China). Tom20 was amplified from Tom20-Emerald (#54282, Addgene, USA). The sequence of mGFP-NES-PABP was amplified from GFP-PASS. H2B was amplified from H2B-GFP (#11680, Addgene, USA)

For cpLOV2-based sensor, we first synthesized cpLOV2 sequence of which the Jα helix contained a NES sequence. To replace different NES, we inserted two BsmBI sites into both ends of NES. cpLOV2, together with mCherry-NLS, was then cloned into linearized pLenti-MCS-GFP-SV40-Puro empty vector. This framework (pLenti-cpLOV2-mCherry-NLS) was further modified by the replacement of mCherry-NLS with NLS-mGFP-NES-PABP, namely Opto-PASSc in this study. We also constructed red Opto-PASSc probe by the replacement of mGFP with mCherry sequence. PABP 4E mutations were introduced into the PABP sequence by primers and its PCR fragment, together with cpLOV2-NLS-mCherry-NES fragment, was inserted into corresponding linearized pLenti-MCS-GFP-SV40-Puro. Opto-PIP3Sc was created by the replacement of PABP region with indicated copies of PH_{BTK} domain from PH-Btk-GFP (#51463, Addgene, USA).

The PI4P sensor based on optically-controlled phase separation was created by fusion of P4M domian from mCherry-P4M-SidM (#51471, Addgene, USA) to mGFP-CIBN. The mGFP (Emerald) was amplified from Tom20-Emerald (#54282, Addgene, USA) and the CIBN was amplified from Tom20-Emerald (#79574, Addgene, USA). The mCherry-CRY2 was amplified as described previously. HOTag3 and HOTag6 was synthesized (Beijing Tsingke Biotech Co., Ltd. China) with corresponding homologous sequence in both ends and a sequence encoding a specific linker. They were subcloned into linearized vector with $(P4M)_n$-mGFP-CIBN and mCh-CRY2, respectively. The above plasmids were assembled with the corresponding purified PCR fragments via Gibson Assembly kit. The sequence and source of other constructions used in this study are listed in Supplementary Materials and all plasmids used in this study were sequenced for validation.

The cell culture and transfection

Cancer cell lines HeLa, COS-7 and 293T used in our research were purchased from ATCC. 293T cell were routinely grown in Dulbecco's Modified Essential Media (DMEM, Hyclone), while HeLa cells were routinely grown in RPMI 1640. The complete medium was supplemented with 10% fetal bovine serum (PAN,

PAN-Biotech, Germany) and 100 U/ml penicillin/streptomycin (Beyotime Biotechnology, China). The cells were cultured at 37 °C in a humidified atmosphere with 5% CO_2. For transient over-expression assay, the cells were plated on confocal dishes. About 1-2 μg indicated plasmid was used according to the instruction of lipofectamine 3000 (Thermo Fisher Scientific, USA).

Living cell imaging

Cells were plated on the confocal dish and then were co-transfected with indicated plasmid. After 24-hour transfection, refreshed with the phenol-free medium. The confocal images were obtained using a AX confocal laser scanning microscope (Nikon, Japan) equipped with a 60×/1.49 numerical aperture (NA) oil immersion objective lens. For light-induced PA probe export, the blue light pulse was 10-12 seconds and the 488 laser power was 1 mW. For starvation-induced PA production, the transfected cells were incubated in HEPES buffer (150 mM NaCl, 20 mM HEPES, 5 mM Glucose, 5 mM KCl, 1 mM $MgCl_2$, 1 mM $CaCl_2$, and 0.1% BSA) for four hours and then images were captured by confocal microscope. For the time-scale detection of PA at plasma membrane, such as PMA-induced PA production, the first image was captured under non-stimulation condition and subsequently 10 μL PBS buffer containing 500 μM PMA (P8139, Sigma-Aldrich, USA) was added into the dish carefully. The capture interval was 8 minutes. For time-scale detection of PI4P at plasma membrane, the images were captured by a C2 confocal laser scanning microscope with a TIRF module (Nikon, Japan). The first image was captured and subsequently PAO (P3075, Sigma-Aldrich, USA) with the indicated final concentration was added into the dish carefully. The capture interval was 10 minutes.

The PLD activity detection

The Amplex™ Red Phospholipase D Assay Kit (Thermo Fisher Scientific, USA) was used to detect cellular total PLD activities. Cells were washed by cold PBS three times and lysed with buffer containing 150 mM NaCl, 50 mM Tris-HCl, 1 mM $CaCl_2$, and 1% Triton X-100 on. The lysates were centrifuged (10 000 rpm/min, 10 min, 4 °C) and the supernatant was used for PLD activity detection according to the

manufactory's instruction.

Statistical analysis

The fluorescence intensity of the images was analyzed by FiJi Image J software (Version 1.53t). Two experimental groups were analyzed by Student's *t*-test (one-tail test). Multigroup comparisons were performed by the one-way ANOVA with Tukey's post hoc test. The *p* values less than 0.05 were considered as significant. Replicates consist of at least three independent experiments. GraphPad Prism were used for data analysis and plot.

Acknowledgements

We thank Prof. Guangwei Du for the gifts RFP-PASS and GFP-PASS. This research was supported by the National key research and development program (2021YFC2101001), the Cross Scientific Research Fund of Zhejiang University of Technology (2022JCY27) and the Natural Science Foundation of Zhejiang Province (LY18H070004).

Ethics declarations

The other authors declare no competing interests.

Contributions

Y.Y, X.L., and L.H. conceived the idea of optogenetic strategies for improvement of biosensors and discussed the optimization of opto-biosensors. H.L., L.H., Y.X., and P.Z. supervised the research. Y.Y, and X.L. designed and conducted most of the experiments. J.L., J.L., Y.C., S.C, T.Z., and S.K. prepared the samples. Y.Y, X.L., J.J. and L.Z. analyzed the experimental data and plotted figures. Y.Y, H.L., L.H., and Y.X. wrote and revised the paper with input from all authors.

References

1. Wang, H. et al. LOVTRAP: an optogenetic system for photoinduced protein dissociation. *Nature methods* **13**, 755-758 (2016).
2. He, L. et al. Circularly permuted LOV2 as a modular photoswitch for optogenetic engineering. *Nature Chemical Biology* **17**, 915-923 (2021).
3. Yumerefendi, H. et al. Light-induced nuclear export reveals rapid dynamics of epigenetic modifications. *Nature Chemical Biology* **12**, 399-401 (2016).
4. Strickland, D. et al. TULIPs: tunable, light-controlled interacting protein tags for cell biology. *Nature methods* **9**, 379-384 (2012).

5. Guntas, G. et al. Engineering an improved light-induced dimer (iLID) for controlling the localization and activity of signaling proteins. *Proceedings of the National Academy of Sciences* **112**, 112-117 (2015).
6. Liu, R. et al. Optogenetic control of RNA function and metabolism using engineered light-switchable RNA-binding proteins. *Nature Biotechnology* **40**, 779-786 (2022).
7. Kennedy, M.J. et al. Rapid blue-light–mediated induction of protein interactions in living cells. *Nature Methods* **7**, 973-975 (2010).
8. He, L. et al. Engineering of a bona fide light-operated calcium channel. *Nature Communications* **12**, 164 (2021).
9. Li, T. et al. A synthetic BRET-based optogenetic device for pulsatile transgene expression enabling glucose homeostasis in mice. *Nature Communications* **12**, 615 (2021).
10. Zhou, Y. et al. A small and highly sensitive red/far-red optogenetic switch for applications in mammals. *Nature Biotechnology* **40**, 262-272 (2022).
11. Yu, Y. et al. Engineering a far-red light–activated split-Cas9 system for remote-controlled genome editing of internal organs and tumors. *Science Advances* **6**, eabb1777 (2020).
12. Deisseroth, K. & Hegemann, P. The form and function of channelrhodopsin. *Science* **357**, eaan5544 (2017).
13. Duan, L. et al. Optogenetic Control of Molecular Motors and Organelle Distributions in Cells. *Chemistry & Biology* **22**, 671-682 (2015).
14. van Bergeijk, P., Adrian, M., Hoogenraad, C.C. & Kapitein, L.C. Optogenetic control of organelle transport and positioning. *Nature* **518**, 111-114 (2015).
15. Zhang, Q. et al. Visualizing Dynamics of Cell Signaling In Vivo with a Phase Separation-Based Kinase Reporter. *Mol Cell* **69**, 334-346.e334 (2018).
16. Li, X., Combs, J.D., Salaita, K. & Shu, X. Polarized focal adhesion kinase activity within a focal adhesion during cell migration. *Nature Chemical Biology* (2023).
17. Li, X. et al. ATM-SPARK: A GFP phase separation–based activity reporter of ATM. *Science Advances* **9**, eade3760 (2023).
18. Tan, P. et al. Optical control of protein delivery and partitioning in the nucleolus. *Nucleic Acids Research* **50**, e69-e69 (2022).
19. Bumpus, T.W. & Baskin, J.M. Clickable substrate mimics enable imaging of phospholipase D activity. *ACS central science* **3**, 1070-1077 (2017).
20. Liang, D. et al. A real-time, click chemistry imaging approach reveals stimulus-specific subcellular locations of phospholipase D activity. *Proc Natl Acad Sci U S A* **116**, 15453-15462 (2019).
21. Tei, R. & Baskin, J.M. Spatiotemporal control of phosphatidic acid signaling with optogenetic, engineered phospholipase Ds. *Journal of Cell Biology* **219** (2020).
22. Bumpus, T.W., Huang, S., Tei, R. & Baskin, J.M. Click chemistry-enabled CRISPR screening reveals GSK3 as a regulator of PLD signaling. *Proc Natl Acad Sci U S A* **118** (2021).
23. Tei, R., Bagde, S.R., Fromme, J.C. & Baskin, J.M. Activity-based directed evolution of a membrane editor in mammalian cells. *Nature Chemistry* **15**, 1030-1039 (2023).
24. Zhang, F. et al. Temporal Production of the Signaling Lipid Phosphatidic Acid by Phospholipase D2 Determines the Output of Extracellular Signal-Regulated Kinase Signaling in Cancer Cells. *Molecular and Cellular Biology* **34**, 84-95 (2014).
25. Kassas, N. et al. Comparative Characterization of Phosphatidic Acid Sensors and Their

Localization during Frustrated Phagocytosis. *J Biol Chem* **292**, 4266-4279 (2017).
26. Yao, Y. et al. Structural insights into phospholipase D function. *Progress in Lipid Research* **81**, 101070 (2021).
27. Sung, T.-C., Altshuller, Y.M., Morris, A.J. & Frohman, M.A. Molecular analysis of mammalian phospholipase D2. *Journal of Biological Chemistry* **274**, 494-502 (1999).
28. Holland, P. et al. HS1BP3 negatively regulates autophagy by modulation of phosphatidic acid levels. *Nature Communications* **7**, 13889 (2016).
29. Dall'Armi, C. et al. The phospholipase D1 pathway modulates macroautophagy. *Nature Communications* **1**, 142 (2010).
30. Hussain, S.S. et al. RalA and PLD1 promote lipid droplet growth in response to nutrient withdrawal. *Cell Rep* **36**, 109451 (2021).
31. Tanenbaum, M.E., Gilbert, L.A., Qi, L.S., Weissman, J.S. & Vale, R.D. A protein-tagging system for signal amplification in gene expression and fluorescence imaging. *Cell* **159**, 635-646 (2014).
32. Taslimi, A. et al. Optimized second-generation CRY2–CIB dimerizers and photoactivatable Cre recombinase. *Nature Chemical Biology* **12**, 425-430 (2016).
33. Yao, Y. et al. Novel function of biguanides in inhibition of phospholipase D1 expression via a translational mechanism in cancer cells. *Genes Dis* **10**, 1787-1790 (2023).
34. Yao, Y. et al. Phospholipase D as a key modulator of cancer progression. *Biological Reviews* **95**, 911-935 (2020).
35. Foo, S., Cazenave-Gassiot, A., Wenk, M.R. & Oliferenko, S. Diacylglycerol at the inner nuclear membrane fuels nuclear envelope expansion in closed mitosis. *Journal of Cell Science* **136** (2023).
36. Thaller, D.J. et al. Direct binding of ESCRT protein Chm7 to phosphatidic acid–rich membranes at nuclear envelope herniations. *Journal of Cell Biology* **220** (2021).
37. Romanauska, A. & Köhler, A. The Inner Nuclear Membrane Is a Metabolically Active Territory that Generates Nuclear Lipid Droplets. *Cell* **174**, 700-715.e718 (2018).
38. Wang, C., Han, B., Zhou, R. & Zhuang, X. Real-Time Imaging of Translation on Single mRNA Transcripts in Live Cells. *Cell* **165**, 990-1001 (2016).
39. Yan, X., Hoek, Tim A., Vale, Ronald D. & Tanenbaum, Marvin E. Dynamics of Translation of Single mRNA Molecules In Vivo. *Cell* **165**, 976-989 (2016).

Figure legends:

Figure 1: optimizing the biosensor of membrane phospholipids based on LOVTRAP system

a, a schematic diagram illustrating the LOVTRAP-based optimal strategy for sequestering the PA biosensor within the cell nucleus.

b, the intracellular localization of Opto-PASSz under the dark conditions and after light stimulation by co-expression of ZDK-mGFP-NES-PABP and H2B-LOV2 (WT) in HeLa cells and **c**, a quantitative analysis was performed to reflect the light-induced

release of the Opto-PASSz from the nucleus by assessing the changes in fluorescence intensity ratio of the cytosol to the nucleus.

d, a performance comparison of Opto-PASSz and the commonly-used PA probe RFP-PASS on the detection of PA levels at the plasma membrane of 293T cells and **e**, its quantitative analysis by measuring the fluorescence intensity ratio of plasma membrane to the cytosol.

Figure 2: the cpLOV-based optimal strategy for membrane phospholipids biosensors

a, a schematic diagram of the cpLOV-based strategy for improvements of membrane phospholipids biosensors.

b, the intracellular localization of Opto-PASSc (fused with mGFP or mCherry) with RFP-PASS in HeLa cells and **c**, colocalization analysis of Opto-PASSc and RFP-PASS, and **d**, a comparison of the background signal of Opto-PASSc with RFP-PASS.

e, the subcellular distribution of Opto-PASSc with wild-type or mutated NES2 in HeLa cells and **f**, to assess the impact of NES2 mutations on background signals, we measured the fluorescence intensity ratio of the cytosol to the nucleus. This analysis involved comparing the following groups: wild-type NES2 *vs.* NES2 with mutations (mGFP-fused) and wild-type NES2 *vs.* NES2 with mutations (mCherry-fused).

g, a quantitative comparison of the nuclear export of Opto-PASSc with wild-type or mutated NES2 in responsive to light stimulation.

h, a quantitative analysis of the detection performance of GFP-PASS probe and our Opto-PASSc with indicated copies of PABP through measuring the fluorescence intensity ratio of plasma membrane to the cytosol.

Figure 3: Opto-PASSc demonstrated superior performance over PASS in detecting PA levels at the nuclear envelope.

a, Opto-PASSc exhibited distinct nuclear envelope localization in various cell lines, whereas RFP-PASS did not and **b**, the fluorescence distribution histogram along the indicated line was utilized to visualize nuclear membrane PA levels labeled with

Opto-PASSc.

c, co-expression of Opto-PASSc (NES2 WT) with both wild-type and mutated PABP motifs in HeLa cells and **d**, co-expression of Opto-PASSc with wild-type NES2 and PABP, as well as Opto-PASSc with mutated NES2 and PABP, in both HeLa and 293T cells , collectively revealed specific PA binding at the nuclear envelope.

Figure 4: improvement of biosensors based on the optically-controlled phase separation

a, a schematic diagram illustrating optically-controlled phase separation for optimizing membrane phospholipid biosensors.

b, the light-induced binding of CRY2/CIBN triggered the phase separation via HOTag3/HOTag6 in HeLa cells with co-expression of indicated plasmids.

c, insoluble the phase separation puncta slowly disaggregated under dark condition.

d, the histogram reflected the brightness distribution of phase separation spots in relation to the background in HeLa cells with co-expression of indicated plasmids and **e**, their the planar dimensions of phase separation puncta.

f, the representative images of phase separation puncta depicted the distribution of PI4P on the plasma membrane after light stimulation in HeLa cells and **g**, the speed histogram reflects the movement of these puncta, and **h**, the trajectory plot of a representative phase separation punctum.

i, the representative images demonstrated an improved resolution in PI4P detection at the plasma membrane.

j, the enhanced probe was employed to monitor PI4P changes on the plasma membrane after a half-hour treatment with a PAO inhibitor.

Supplementary figure 1: Optogenetic strategies based on optogenetic elements LOVTRAP for optimizing PA biosensors

a, the colocalization of GFP-PLD2 and the CRY2-based PA biosensor with one copy or two copies (**b**) of PABP motif from SPO20.

c, a schematic diagram illustrating the LOVTRAP-based optimal strategy for trapping

the PA biosensor onto the mitochondrial.

d, the redesigned probe Opto-PASSz was released from the mitochondrial and diffused into the cytosol after blue light stimulation and **e**, the quantitative analysis of this process by measuring the fluorescence intensity ratio of mitochondrial to the cytosol.

Supplementary figure 2: Screening of NES for regulating the nuclear export of cpLOV2 and evaluation of the PA binding motif among various PA binding proteins

a, the design of cpLOV-based nucleocytoplasmic transport with various NES sequence and **d**, representative images of cpLOV-mCh-NLS distribution in cells under non-stimulation condition and quantitative analysis of the light-induced nuclear export of cpLOV-mCh-NLS with fusion of different NES sequences.

c, the schematic diagram of the cpLOV-based PA biosensor (Opto-PASSc) with two PABP motifs from yeast Opi1p and **d**, representative images of co-expression of Opto-PASSc with RFP-PASS or mCh-PLD2 in HeLa cells, and **e**, co-expression of Opto-PASSc with RFP-PASS in 293T cells.

f, the sequence design of the Opto-PASSc with three PABP motifs from Raf1 protein and **g**, representative images of its co-expression with mCh-PLD2.

h, representative images and quantitative analysis of the co-expression of Opto-PASSc with mCherry-PASS (both fused two PABP motifs from SPO20).

i, representative images of the co-expression of Opto-PASSz and Opto-PASSc.

j, the sequence of PABP 4E mutation and the co-expression of Opto-PASSc with and without PABP 4E mutation.

Supplementary figure 3: comparing the detection performance of Opto-PIP3Sc and Opto-PI4PSc, and assessing Opto-PASSc for detecting plasma membrane PA levels.

a, the sequence design and representative images of the cpLOV-based PIP3 biosensor and **b**, representative images and quantitative analysis (**c**) of demonstrated an improved detection performance for plasma membrane PI4P.

d-k, the PA detection by Opto-PASSc with indicated copies of PABP motifs and RFP-PASS in the PLD2-overexpressed (PLD2 wild type or inactive mutation) and **l**, co-expression of PLD2 (WT) and Opto-PASSc in HeLa cells after FIPI treatment.

m, representative images and analysis of the detection performance of GFP-fused and mCherry-fused Opto-PASSc.

Supplementary figure 4: Opto-PASSc outperformed PASS at PA labeling under different stimulations

a, the detection performance of Opto-PASSc and RFP-PASS at varying expression levels in response to PMA-induced PA increase, and the quantitative analysis of the SNR of both probes (**b**).

c, quantitative analysis of the fluorescence intensity ratio of plasma membrane to the cytosol after 5 μM PMA treatment in HeLa cells with co-expression of Opto-PASSc and RFP-PASS.

d, Opto-PASSc clearly labelled PA at plasma membrane and its analysis (**e**) of the fluorescence intensity ratio of plasma membrane to the cytoplasm in 293T cells under basal state, and **f**, the chemical assay compared the basal PLD activities between HeLa and 293T cells.

g, the PA detection of Opto-PASSc and RFP-PASS in HeLa cells after four-hour starvation in HEPES buffer and **h**, quantitative analysis of the the fluorescence intensity ratio of plasma membrane to the cytoplasm for Opto-PASSc with different copies of PABP motifs.

i, blue light illumination enhanced the performance of Opto-PASSc in response to PMA stimulation.

Supplementary figure 5: the optically-controlled phase separation improved the detection resolution of PI4P biosensor

a, the representative image of the phase separation foci in the HeLa cells with exchange of HOTag3 and HOTag6 to corresponding proteins (P4M-mGFP-CIBN-HOTag6 and mCh-CRY2-HOTag3) before and after light stimulation.

b, the representative image of the phase separation foci from the red channel (mCh-CRY2-HOTag6) under indicated treatments.

c, the optically-controlled phase separation improved the detection resolution of PI4P biosensor at the plasma membrane in HeLa cells and its analysis (**d**).

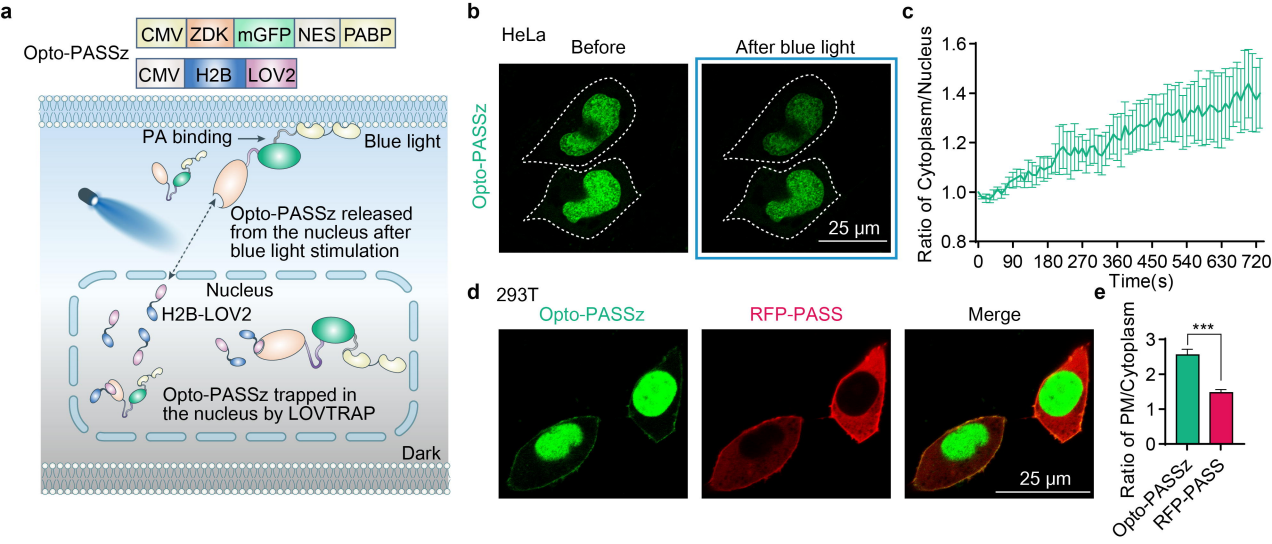
a
Opto-PASSz
CMV
ZDK
mGFP
NES
PABP
CMV
H2B
LOV2
PA binding
Blue light
Opto-PASSz released from the nucleus after blue light stimulation
Nucleus
H2B-LOV2
Opto-PASSz trapped in the nucleus by LOVTRAP
Dark
b
HeLa
Before
After blue light
Opto-PASSz
25 μm
c
Ratio of Cytoplasm/Nucleus
1.6
1.4
1.2
1.0
0.8
0
90
180
270
360
450
540
630
720
Time(s)
d
293T
Opto-PASSz
RFP-PASS
Merge
25 μm
e
Ratio of PM/Cytoplasm
3
2
1
0
***
Opto-PASSz
RFP-PASS

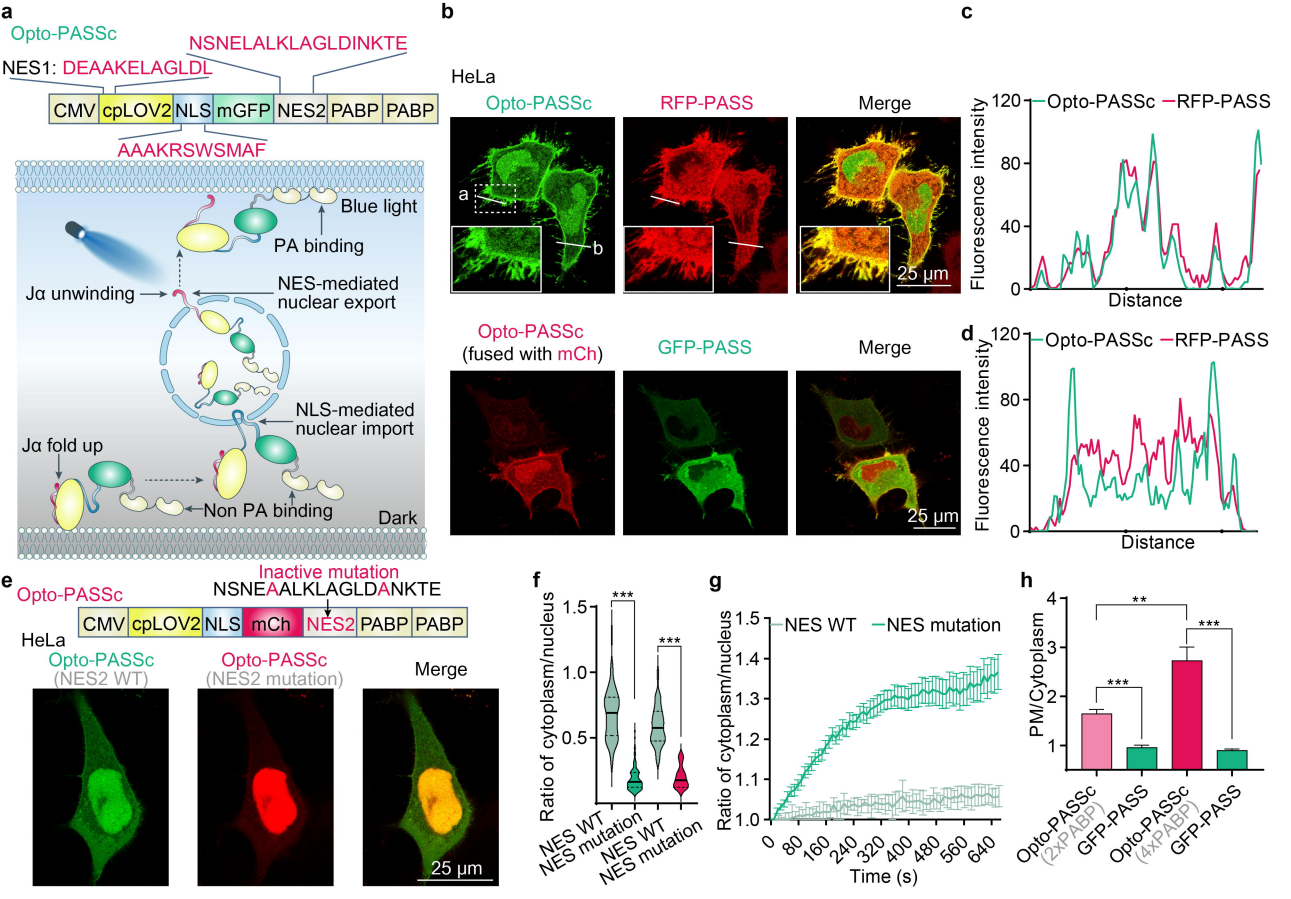
a
Opto-PASSc
NSNELALKLAGLDINKTE
NES1: DEAAKELAGLDL
CMV
cpLOV2
NLS
mGFP
NES2
PABP
PABP
AAAKRSWSMAF
Blue light
PA binding
Jα unwinding
NES-mediated nuclear export
NLS-mediated nuclear import
Jα fold up
Non PA binding
Dark
b
HeLa
Opto-PASSc
RFP-PASS
Merge
a
b
25 μm
Opto-PASSc (fused with mCh)
GFP-PASS
Merge
25 μm
c
Opto-PASSc
RFP-PASS
Fluorescence intensity
Distance
d
Opto-PASSc
RFP-PASS
Fluorescence intensity
Distance
e
Opto-PASSc
Inactive mutation
NSNEAALKLAGLDANKTE
CMV
cpLOV2
NLS
mCh
NES2
PABP
PABP
HeLa
Opto-PASSc (NES2 WT)
Opto-PASSc (NES2 mutation)
Merge
25 μm
f
Ratio of cytoplasm/nucleus
***
***
NES WT
NES mutation
NES WT
NES mutation
g
NES WT
NES mutation
Ratio of cytoplasm/nucleus
Time (s)
h
PM/Cytoplasm
**
***
***
Opto-PASSc (2xPABP)
GFP-PASS
Opto-PASSc (4xPABP)
GFP-PASS

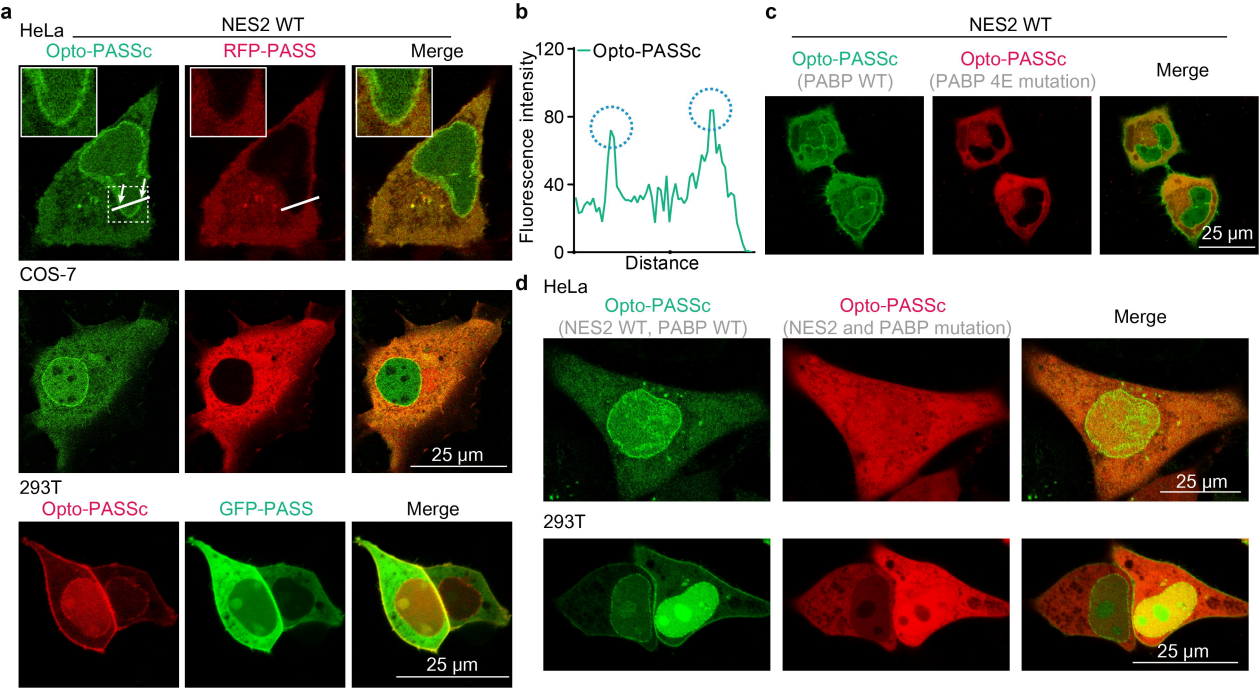
a
HeLa
NES2 WT
Opto-PASSc
RFP-PASS
Merge
COS-7
25 μm
293T
Opto-PASSc
GFP-PASS
Merge
25 μm
b
Opto-PASSc
Fluorescence intensity
120
80
40
0
Distance
c
NES2 WT
Opto-PASSc
(PABP WT)
Opto-PASSc
(PABP 4E mutation)
Merge
25 μm
d
HeLa
Opto-PASSc
(NES2 WT, PABP WT)
Opto-PASSc
(NES2 and PABP mutation)
Merge
25 μm
293T
25 μm

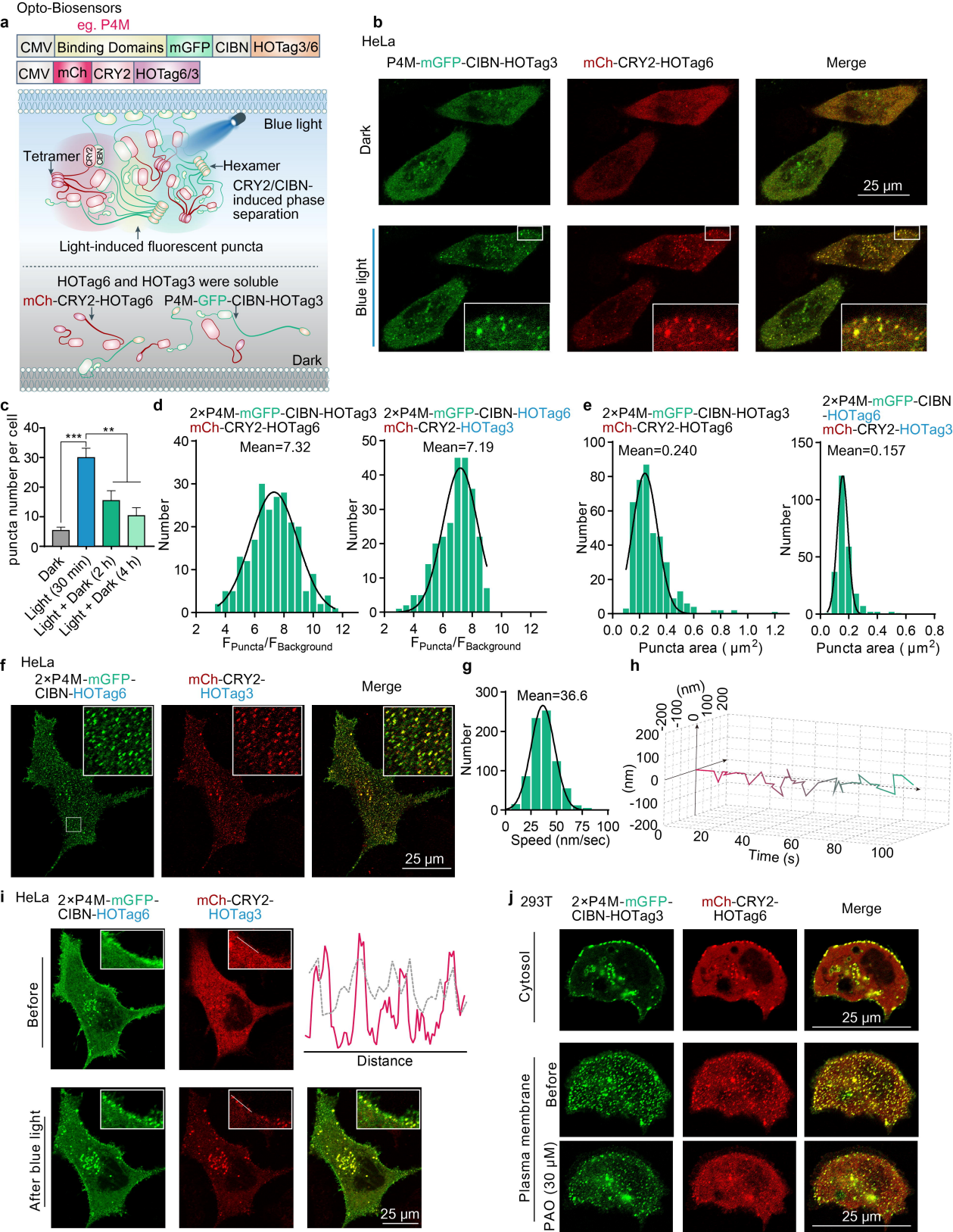
a
Opto-Biosensors
eg. P4M
CMV
Binding Domains
mGFP
CIBN
HOTag3/6
CMV
mCh
CRY2
HOTag6/3
Blue light
Tetramer
CRY2
CIBN
Hexamer
CRY2/CIBN-induced phase separation
Light-induced fluorescent puncta
HOTag6 and HOTag3 were soluble
mCh-CRY2-HOTag6
P4M-GFP-CIBN-HOTag3
Dark
b
HeLa
P4M-mGFP-CIBN-HOTag3
mCh-CRY2-HOTag6
Merge
Dark
Blue light
25 μm
c
puncta number per cell
***
**
Dark
Light (30 min)
Light + Dark (2 h)
Light + Dark (4 h)
d
2×P4M-mGFP-CIBN-HOTag3
mCh-CRY2-HOTag6
Mean=7.32
2×P4M-mGFP-CIBN-HOTag6
mCh-CRY2-HOTag3
Mean=7.19
Number
F_Puncta/F_Background
e
2×P4M-mGFP-CIBN-HOTag3
mCh-CRY2-HOTag6
Mean=0.240
2×P4M-mGFP-CIBN-HOTag6
mCh-CRY2-HOTag3
Mean=0.157
Number
Puncta area (μm²)
f
HeLa
2×P4M-mGFP-CIBN-HOTag6
mCh-CRY2-HOTag3
Merge
25 μm
g
Mean=36.6
Number
Speed (nm/sec)
h
(nm)
Time (s)
i
HeLa
2×P4M-mGFP-CIBN-HOTag6
mCh-CRY2-HOTag3
Before
After blue light
Distance
25 μm
j
293T
2×P4M-mGFP-CIBN-HOTag3
mCh-CRY2-HOTag6
Merge
Cytosol
Plasma membrane
Before
PAO (30 μM)
25 μm